Unleashing the Glow: Upconverting Nanoparticles Recharge Persistent Luminescent Materials – applications in 3D-printing and optical coding

Adrian Drozdowski[1], Dirk Poelman[2], Marcin Runowski[1], Hanoch Hemmerich[3], Fernando Rivera-López[4], Tomasz Grzyb[*1]

[1]Department of Rare Earths, Faculty of Chemistry, Adam Mickiewicz University, Poznan, Poland

[2]Lumilab, Department of Solid State Sciences, Faculty of Sciences, Ghent University, Ghent, Belgium

[3]Departamento de Física, IUdEA, IMN and MALTA Consolider Team,

Universidad de La Laguna, San Cristóbal de La Laguna E-38200, Santa Cruz de Tenerife, Spain

[4]Departamento de Ingeniería Industrial, Escuela Superior de Ingeniería y Tecnología

Universidad de La Laguna, San Cristóbal de La Laguna E-38200, Santa Cruz de Tenerife, Spain

E-mail: tgrzyb@amu.edu.pl

Persistent luminescence (PersL) materials show long-lasting emission after irradiation with excitation light. Usually, to obtain PersL, excitation with ultraviolet (UV) or visible light is necessary, which limits the use of this phenomenon when the material is in a non-transparent medium for excitation light. A solution to this problem comes from upconverting nanoparticles (UCNPs), which convert near-infrared light, usually not absorbed by such media as polymers or biological tissues, to higher-energetic UV photons, recharging the PersL phosphors. In this article, we report composite materials consisting of PersL phosphor and UCNPs, i.e. $SrAl_2O_4:Eu^{2+}$ or $ZnGa_2O_4:Cr^{3+}$ and upconverting $LiYbF_4:Tm^{3+}@LiYF_4$ core@shell nanoparticles. These materials show dual-emission properties - bright upconversion from near-infrared (NIR at 975 nm) to ultraviolet (UV at 347 nm) and long-lasting PersL in the visible light range. The obtained composite materials present intense, persistent luminescence after the NIR laser excitation. This article proves efficient energy transfer from UCNPs to PersL phosphor and opens new possibilities in the design and synthesis of composite materials. By employing the high-resolution 3D-

printing technology, we experimentally confirmed the possibility of multi-modal optical information storage by applying the synthesized materials, developing multi-dimensional microstructured patterns with QR code, letters and first bi-modal, single- and double-layered 8-bit codes based on the combination of PersL and upconversion emission.

Keywords: upconversion, persistent luminescence, nanoparticles, lanthanides, optical coding

Introduction

Persistent luminescence (PersL), also called "afterglow", has been known for a long time.[1–3] It is a phenomenon of materials showing long-lasting luminescence, typically from minutes to hours after the end of irradiation. These materials have been widely used in glow-in-dark toys and safety signs since the last decades of the XXth century.[4] Currently, studies around PersL focus on many areas, such as bioimaging,[5] X-ray detection,[6] dosimetry,[7] photodynamic therapy,[8] anti-counterfeiting,[9] optical data storage and coding.[10,11] Long-lasting luminescent nanoparticles with efficient near-infrared (NIR) emission have been intensively investigated recently, emerging as a new generation of probes for *in vivo* optical imaging.[12,13] PersL allows for separating the excitation and emission process by irradiating nanoparticles (NPs) externally before injecting them into the organism.[14,15] Recently, tomographic imaging based on PersL has been proposed, showing higher resolution and deeper imaging than classical fluorescence imaging.[14]

However, PersL materials require ultraviolet (UV) or visible (Vis) excitation before use.[8] Usually, the material or biomaterial used as a carrier for PersL phosphor strongly absorbs light in the UV-Vis range, which has harmful properties that lead to photochemical reactions and carrier degradation. In extreme situations, this makes it impossible to recharge PersL materials. On the other hand, NIR radiation can easily penetrate various materials, including polymers and biological tissues.[16,17] The possibility of NIR to Vis conversion allows for the broad application of upconverting nanoparticles (UCNPs) in anti-counterfeiting, optical information storage, bioimaging, biosensors, and photodynamic therapy.[18–28] Thus, combining PersL materials and

UCNPs could lead to many new applications.[12,29] Moreover, creating these composite materials would address a crucial challenge faced by current PersL materials in biomedical applications - the ability to recharge them once integrated into biological materials.

So far, only a few studies have reported successful excitation of PersL materials using NIR light. However, these reports presented materials based on PersL phosphors (glass, bulk, or nanomaterials) doped with appropriate lanthanide ions to achieve upconversion (UC).[12,29–32] The new way to obtain PersL-UC hybrid materials would be by covering UCNPs with PersL phosphors to obtain hybrid UC nanophosphors. The first step in this approach should be proving that efficient radiation energy transfer between the UCNPs and PersL material is possible. In order to do so, appropriate UCNPs and PersL phosphors should be chosen.

The most popular and studied material for PersL is $SrAl_2O_4$ doped with Eu^{2+} and Dy^{3+} ions.[33–36] Researchers reported numerous methods for synthesizing PersL phosphors, yielding various forms, such as bulk materials, glass ceramics, and NPs.[37,38] The popularity of $SrAl_2O_4$-based materials derives from several unique properties, such as bright and highly long-lasting luminescence, up to several hours or even days.[34,39] Another advantage is that the maximum emission localized is around 520 nm, which is seen well by the human eye (as a green colour), with the possibility of tuning it, e.g., by doping with different ions. Moreover, the wide absorption band from deep UV to even blue spectral range enables charging the material with solar daylight and artificial lighting inside buildings.[37]

Another group of highly investigated PersL phosphors, especially for bioapplications, are materials doped with Cr^{3+} ions, for example, $ZnGa_2O_4$.[40–43] Their popularity derives from the location of the PersL emission band of Cr^{3+} ions, around 700 nm in the first biological window range.[44,45] This property allows for multiple applications of such materials in bioimaging and photodynamic therapy.[46,47]

A critical aspect of designing new hybrid PersL-UC phosphors is using adequate UCNPs for the PersL material excitation. The UC emission bands of the NPs should correspond to the excitation range of the PersL phosphor to enable efficient reabsorption and recharging. UV light

can charge most of the PersL materials. Because of that, the UCNPs should exhibit intense UV emission under NIR excitation.

Due to the low phonon energy, fluorides are among the most promising UCNPs for NIR to UV conversion. Usually, their phonon energy is lower than 400 cm^{-1}.[48] Recently, the highly investigated materials showing such UC properties are UCNPs based on $NaYF_4$ or $LiYF_4$ doped with Tm^{3+} ions and covered with an inert shell, composed of the material forming host of the cores.[20,49–53] However, in hexagonal, $NaYF_4$-based materials, most light is emitted in the visible range.[54] $LiYF_4$-based materials present different spectroscopic properties because of the tetragonal crystal structure, and typically, they show brighter emission in the UV range, depending on the concentration of Tm^{3+} dopant ions. We have chosen $LiYbF_4$:Tm^{3+}@$LiYF_4$ core@shell UCNPs in our research because of their bright emission in the UV range, which we investigated previously.[20]

This work presents the spectroscopic properties of new composite materials resulting from the combination of the $LiYbF_4$:Tm^{3+}@$LiYF_4$ UCNPs with two distinct PersL phosphors: $SrAl_2O_4$:Eu^{2+},Dy^{3+}, or $ZnGa_2O_4$:Cr^{3+}. We confirmed a successful realization of energy transfer from the UCNPs to the PersL materials in the fabricated composites, *i.e.* by reabsorption of UV light emitted from the UCNPs and its consequent ability to charge the PersL phase, thereby enabling NIR excitation of these composite materials. Thanks to highly efficient afterglow effects and UC luminescence, we could 3D-print several polymer items containing the developed materials, including micron-sized QR codes, letters, and binary codes. Moreover, we show for a first-time realization on a double-layer, multi-dimensional optical coding platform operating with combined afterglow and UC modes, allowing high-capacity optical information loading and their decoding *via* an 8-bit ASCII system.

Experimental section

Materials and methods

For UCNPs synthesis, we used the following reagents: Y_2O_3, Tm_2O_3, and Yb_2O_3 (all with 99.99% purity, Alfa Aesar, Germany), lithium chloride (99%, Acros Organics, Poland), ammonium fluoride (99.99%, Merck, Poland), n-hexane (≥99%, Honeywell, Poland), ethanol (99.8%, Avantor, Poland), oleic acid (OA; 90%) and tri-n-octylamine (TOA; 95%) from Alfa Aesar (Germany), hydrochloric acid (37%) and sodium oleate (82%) from Merck (Poland). For the solid-state synthesis of PersL phosphors, we used the following chemicals: Al_2O_3, Cr_2O_3, ZnO, Ga_2O_3, and $SrCO_3$ (99.99%, Alfa Aesar, Germany), EuF_3 and DyF_3 (Sigma Aldrich, Germany) and boric acid (H_3BO_3, >99.8%, Honeywell).

For powder X-ray diffraction measurements, a Siemens D5000 diffractometer (40 kV, 40 mA) with Cu Kα1 radiation (λ = 0.154 nm) was used. Scanning electron microscope (SEM) imaging was performed using a Hitachi S-3400N microscope under a pressure of 25 Pa and an accelerating voltage of 20 kV to avoid sample charging. The obtained materials' excitation and emission spectra were measured using an Edinburgh FS920 (Edinburgh Instruments Ltd., Livingston, UK) fluorescence spectrometer equipped with a monochromate 450 W Xe-arc lamp as the excitation source. For persistent luminescence measurements, a light-emitting diode centred at 375 nm or CNI 50 mW 375 nm laser was used with a calibrated photopic ILT1700 detector from International Light for visible emission and a photosensor amplifier C9329-01 from Hamamatsu Photonics coupled to a large area Si photodiode for measurements in the NIR range. Because of the non-exponential character of luminescence decays, the below equation was used for PersL lifetimes calculations:[55]

$$\tau = \frac{\int_0^\infty tI(t)dt}{\int_0^\infty I(t)dt}$$

where τ is the decay time, and $I(t)$ is the intensity at time t.

Synthesis of core UCNPs

$LiYbF_4$:0.5%Tm^{3+}@$LiYF_4$ core@shell UCNPs were synthesized based on our previous report using the two-step coprecipitation method in high-temperature boiling solvents.[20] Also, the concentration of Tm^{3+}, giving the highest emission intensity in the UV range, was selected based on previous reports.[20,56] Concentrations 0.2% or 1% of Tm^{3+} ions also provide UV emission but with lower intensity than 0.5%.[20] As precursors, we used lanthanide oleates (for more details, see Supplementary Information - SI). We performed all operations in a Schlenk line, maintaining a nitrogen gas atmosphere or working under a vacuum ($<10^{-2}$ mbar). For a typical synthesis of 1 mmol of core NPs - $LiYbF_4$:0.5%Tm^{3+}, lithium chloride (1 mmol), thulium and ytterbium oleates (1 mmol in total), trioctylamine (TOA, 12 mL), and OA (oleic acid, 8 mL) were mixed in a three-neck round bottom flask. The mixture was then degasified for one hour under a vacuum at 130 °C. Then, the temperature was increased to 160 °C, and the stirring continued for 30 minutes in a nitrogen gas atmosphere. The mixture was cooled to 100 °C in the next step to add solid ammonium fluoride (4 mmol). Immediately after that, the mixture was again outgassed for 10 minutes while maintaining the 100 °C temperature. Finally, the mixture was heated at 320 °C for one hour under nitrogen gas flow. After cooling to room temperature, core NPs were isolated using centrifugation and washed with ethanol for purification (see SI for more details).

Synthesis of core@shell UCNPs

The core@shell NPs ($LiYbF_4$:0.5%Tm^{3+}@$LiYF_4$) synthesis protocol was similar to that of the core NPs. Initially, we mixed 2 mmol of lithium chloride and 2 mmol of yttrium oleate with 36 mL of trioctylamine (TOA) and 24 mL of oleylamine (OA). Subsequently, the mixture was outgassed at 100 °C for 1 h and cooled down to 60 °C, and then it was mixed with the previously synthesized hexane colloid of the core NPs (1 mmol). Next, the solution was stirred at 130 °C under nitrogen gas flow for 30 minutes and then under vacuum for another 30 minutes. After cooling the mixture to 100 °C, we added 2 mmol of ammonium fluoride, and the entire mixture was degasified, following a procedure similar to that used in the core synthesis. Finally, we conducted the reaction at 280 °C for 80 minutes under a nitrogen gas flow. After cooling the

mixture to room temperature, we isolated the core@shell UCNPs following the procedure described in the SI file.

Synthesis of $SrAl_2O_4:Eu^{2+},Dy^{3+}$

We obtained the PersL phosphor $SrAl_2O_4$:1%Eu^{2+},0.5%Dy^{3+} *via* the solid-state synthesis method.[57] Al_2O_3 and $SrCO_3$ precursors were homogenously mixed in an agate mortar in the ½:1 molar ratio with EuF_3 and DyF_3 (1% and 0.5% mol of Al^{3+} ions, respectively). Subsequently, 0.4 wt.% of H_3BO_3 was added as a flux. Then, the entire mixture was ground in a mortar for 30 minutes. Afterwards, the material was placed in the tube furnace in a reducing atmosphere (N_2/10% H_2) and heated for 4 hours at 1350 °C. After cooling to room temperature, the material was ground again in an agate mortar and analysed further.

Synthesis of $ZnGa_2O_4:Cr^{3+}$

The method of solid-state synthesis of $ZnGa_2O_4$:0.5%Cr^{3+} was reported previously.[40] In the first step, we mixed metal oxides (ZnO, Ga_2O_3) in the 1:½ ratio with Cr_2O_3 in the 0.5% mol amount regarding Ga_2O_3. Next, the powders were mixed with 10 mL of ethanol and ground in a ball mill for one hour at 300 RPM using nine ZrO_2 balls. After that, we heated the resulting mixture to 60 °C to evaporate ethanol. Further, the sample was heated in an oven for 4 hours at 1000 °C in air. After cooling down, the sample was again ground in an agate mortar into a powder and taken for further analysis.

Preparation of PersL-UC composite materials

The corresponding composite materials were obtained by mixing solid core@shell UCNPs with PersL phosphors $SrAl_2O_4:Eu^{2+},Dy^{3+}$ or $ZnGa_2O_4:Cr^{3+}$ at a 1:1 wt. ratio, together with 10 mL of ethanol (for 1g of mixed powders). Next, we transferred the mixture to a planetary ball mill and ground the sample for 1 hour at 300 rpm using nine ZrO_2 balls. Afterwards, we heated the entire mixture at 60 °C to evaporate ethanol. Finally, we took the resulting powder composite materials for further analysis. In the end, two composites were obtained: $SrAl_2O_4:Eu^{2+},Dy^{3+}$ with UCNPs (SAO-UCNPs) and $ZnGa_2O_4:Cr^{3+}$ with UCNPs (ZGO-UCNPs).

Results and discussion

Structural characterization

We used powder X-ray diffraction analysis (XRD) to investigate the structure of the synthesized compounds and prepare composite materials. Fig. 1 presents XRD patterns of synthesized materials, including $LiYbF_4$:0.5%Tm^{3+}@$LiYF_4$ core@shell NPs (UCNPs), PersL phosphors $SrAl_2O_4$:Eu^{2+},Dy^{3+} (SAO) and $ZnGa_2O_4$:Cr^{3+} (ZGO), PersL-UC composites (SAO-UCNPs and ZGO-UCNPs). The reference patterns for $LiYbF_4$, $SrAl_2O_4$, and $ZnGa_2O_4$ used for comparison are from the Crystallography Open Database (COD). There were no additional peaks in the XRD patterns, and all present patterns matched the reference well. Moreover, according to Sherrer's equation, the broadening of some peaks can be observed in patterns derived from UCNPs due to their small crystallite size [58].

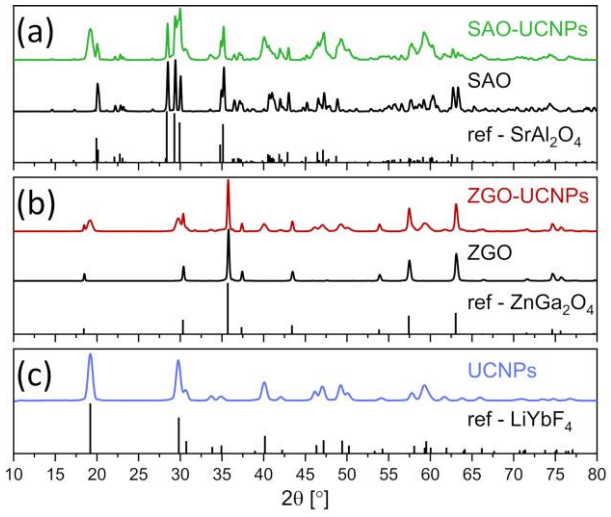

Fig. 1. XRD patterns of obtained materials (a) $SrAl_2O_4$:1%Eu^{2+},0.5%Dy^{3+} (SAO) and composite $SrAl_2O_4$:1%Eu^{2+},0.5%Dy^{3+}-UCNPs, (b) $ZnGa_2O_4$:0.5%Cr^{3+} (ZGO) and the composite $ZnGa_2O_4$:0.5%Cr^{3+}-UCNPs and (c) $LiYbF_4$:0.5%Tm^{3+}@$LiYF_4$ UCNPs. Reference patterns for the pure $SrAl_2O_4$ – 2002284, $ZnGa_2O_4$ – 4001767 and $LiYbF_4$ – 4344179 were taken from the COD database.

For further structure characterization, electron microscopy (TEM and SEM) was used (Fig. 2). Obtained UCNPs were highly monodispersed, and all presented the same shape. The average size of UCNPs was 24.2 ± 3.2 nm in length and 18.5 ± 2.5 nm in width. Additionally, the well-

defined core@shell structure of UCNPs was confirmed using HRTEM microscopy. In the case of obtained PersL phosphors, both samples had a size of several microns and presented one type of structure. After mixing PersL materials with UCNPs, the size of crystallites slightly decreased because of the additional milling step.

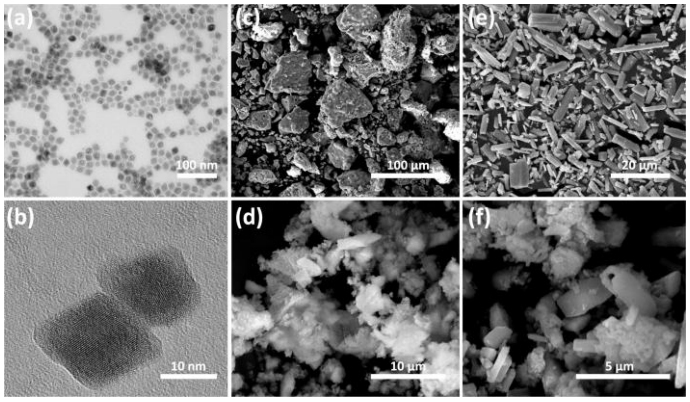

Fig. 2. (a) TEM and (b) HRTEM images of $LiYbF_4$:0.5%Tm^{3+}@$LiYF_4$ UCNPs and SEM images of obtained materials: (c) $SrAl_2O_4$:Eu^{2+},Dy^{3+}, (d) $SrAl_2O_4$:Eu^{2+},Dy^{3+}-UCNPs, (e) $ZnGa_2O_4$:Cr^{3+}, (f) $ZnGa_2O_4$:Cr^{3+}-UCNPs.

Spectroscopic properties

To analyse the spectroscopic properties of the obtained PersL materials, we measured their excitation and emission spectra (Fig. 3). A 375 nm LED was used as an excitation source for emission measurements.

Excitation spectra of the $SrAl_2O_4$:Eu^{2+},Dy^{3+}-based materials presented in Fig. 3a consist of a single, broad band related to the $4f^7(^8S_{7/2}) \rightarrow 4f^65d^1$ transition of Eu^{2+} ions.[59,60] The emission spectra of these samples (Fig. 3b) show a broad band related to the radiative relaxation of Eu^{2+} ions to the $4f^7(^8S_{7/2})$ ground state with a maximum of around 520 nm.[59]

On the other hand, three broad bands are present in the excitation spectra of the $ZnGa_2O_4$:Cr^{3+}-based materials (Fig. 3c). The band in the UV region (with a maximum at around 300 nm) originates from a partial overlap of the $ZnGa_2O_4$ host absorption with the spin-allowed transition of Cr^{3+} ions from the ground state [$^4A_2$ (^4F)] to the excited state [$^4T_1$ (^4P)].[61] The bands observed at approximately 410 and 550 nm are attributed to the spin-allowed transitions of Cr^{3+} ions in an

octahedral symmetry. They originate from the transitions from the ground state [$^4A_2$ (^4F)] to the excited states $^4T_1$ (^4F) and $^4T_2$ (^4F), respectively.[45,61] In the $ZnGa_2O_4$:Cr^{3+}-based materials, the emission spectra (Fig. 3d) show multiple bands at around 700 nm, characteristic of the Cr^{3+} ions embedded in a strong crystal field.[62–64] The bands correspond to the spin-forbidden ^2E (^2G) → $^4A_2$ (^4F) transition of Cr^{3+}. The recorded band consists of multiple components resulting from the crystal field splitting effect and incorporating Cr^{3+} ions into the $ZnGa_2O_4$ structure at two Ga^{3+} sites with different coordination environments.[61]

The intensity of the excitation and emission of both $SrAl_2O_4$:Eu^{2+},Dy^{3+} and $ZnGa_2O_4$:Cr^{3+}-based materials decreased after mixing with UCNPs. This effect is due to the dilution of PersL phosphors with UCNPs, as well as because of light scattering and reabsorption effects.

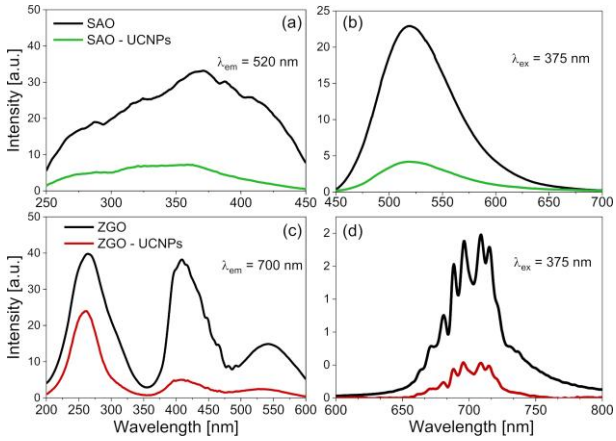

Fig. 3. Excitation (a, c) and emission spectra (b, d) of the obtained materials - $SrAl_2O_4$:1%Eu^{2+},0.5%Dy^{3+} (SAO), $ZnGa_2O_4$:0.5%Cr^{3+} (ZGO), $SrAl_2O_4$:1%Eu^{2+},0.5%Dy^{3+}-UCNPs (SAO-UCNPs) and $ZnGa_2O_4$:0.5%Cr^{3+}-UCNPs (ZGO-UCNPs). Excitation spectra were obtained by monitoring the maxima of the emission at 700 and 520 nm for Cr^{3+} and Eu^{2+}, respectively. Emission spectra were taken under a 375 nm LED excitation source.

Under irradiation with a 975 nm laser (excitation flux of 6 W·cm^{-2}), the studied materials exhibit intense upconversion luminescence presented in Figs. 4 and 5a. All composite materials exhibit lower emission intensities in the whole spectrum compared to the pure UCNPs sample, which corresponds to the lower content of the UCNPs

(50% mass) in the composite materials, compared to the pure UCNPs, as well as due to the previously mentioned light scattering and reabsorption effects. Each tested sample showed the same emission bands deriving from UCNPs, *i.e.* two peaks in the UV region (347 and 362 nm), another three in the visible spectral range (447, 475, and 647 nm), and one the most intense band at around 800 nm located in the NIR region. All recorded bands correspond to the 4f-4f electronic transitions of Tm^{3+} ions, as indicated in Fig. 4.[20] The high emission intensity in the UV range confirms efficient energy transfer between the Yb^{3+} ions and Tm^{3+} emitters. A low concentration of Tm^{3+} ions in the studied UCNPs allowed for minimizing cross-relaxation processes, thus generating intense UC emission in the UV range.[65]

The composite materials show the unique possibility of charging the PersL phosphors by upconversion, so the conversion of NIR excitation photons into green or red afterglow emission. The observed effect is due to the reabsorption of UV light emitted from the UCNPs by $SrAl_2O_4:Eu^{2+},Dy^{3+}$, or $ZnGa_2O_4:Cr^{3+}$ materials, which is seen in Fig. 4 and manifested by a much more significant reduction of the intensity of the UV bands (at 350 nm), compared to other peaks in the visible and NIR ranges. Confirmation of the excitation of the PersL phase *via* upconversion is shown in the next paragraph.

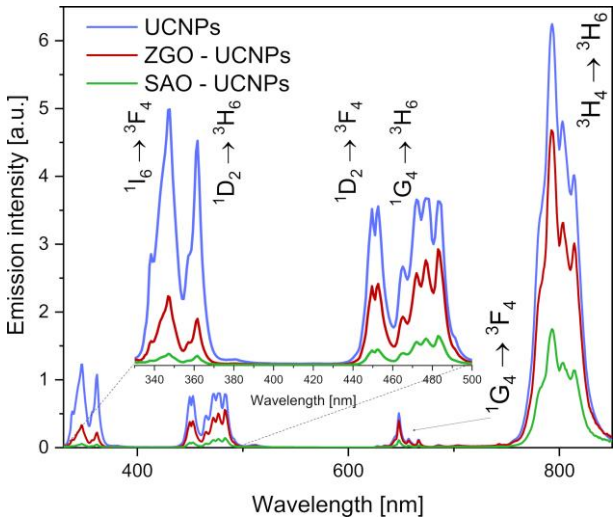

Fig. 4. Emission spectra of the $LiYbF_4:0.5\%Tm^{3+}@LiYF_4$ (UCNPs), $ZnGa_2O_4:0.5\%Cr^{3+}$-UCNPs (ZGO-UCNPs) and $SrAl_2O_4:1\%Eu^{2+},0.5\%Dy^{3+}$-UCNPs (SAO-UCNPs) materials under 975 nm laser excitation with a power density of 6 $W \cdot cm^{-2}$.

Figs. 5c and d demonstrate simplified mechanisms of persistent luminescence, upconversion and postulated radiation energy transfer between two components of the studied composite materials. The SAO and ZGO materials can be excited in two ways – by direct UV irradiation, resulting in their excitation to the conduction band or by UV radiation produced by UCNPs as a consequence of energy transfer between Yb^{3+} and Tm^{3+} and multiphoton excitation of Tm^{3+} ions.[20,66] The excited PersL materials undergo relaxation to the emitting levels of Eu^{2+} or Cr^{3+} ions, or the absorbed energy can be stored in traps and then slowly released to the emitter ions, resulting in emission.[66]

Additionally, photos of samples were taken to present the materials' luminescence properties better. Figs. 5a and 5b. shows all the luminescent properties of obtained materials. All the samples containing UCNPs showed bright blue emission under NIR excitation. Composite samples both showed PersL after the NIR excitation, but as was stated before, in the case of ZGO-UCNPs composite, the luminescence was weaker and thus impossible to record on a photo.

On the other hand, the PersL of all samples was well visible after UV excitation. Additionally, we compare the emission intensity of SAO-based samples over 20 minutes. As can be seen, the well-defined and various spectroscopic properties of obtained materials allow for many applications.

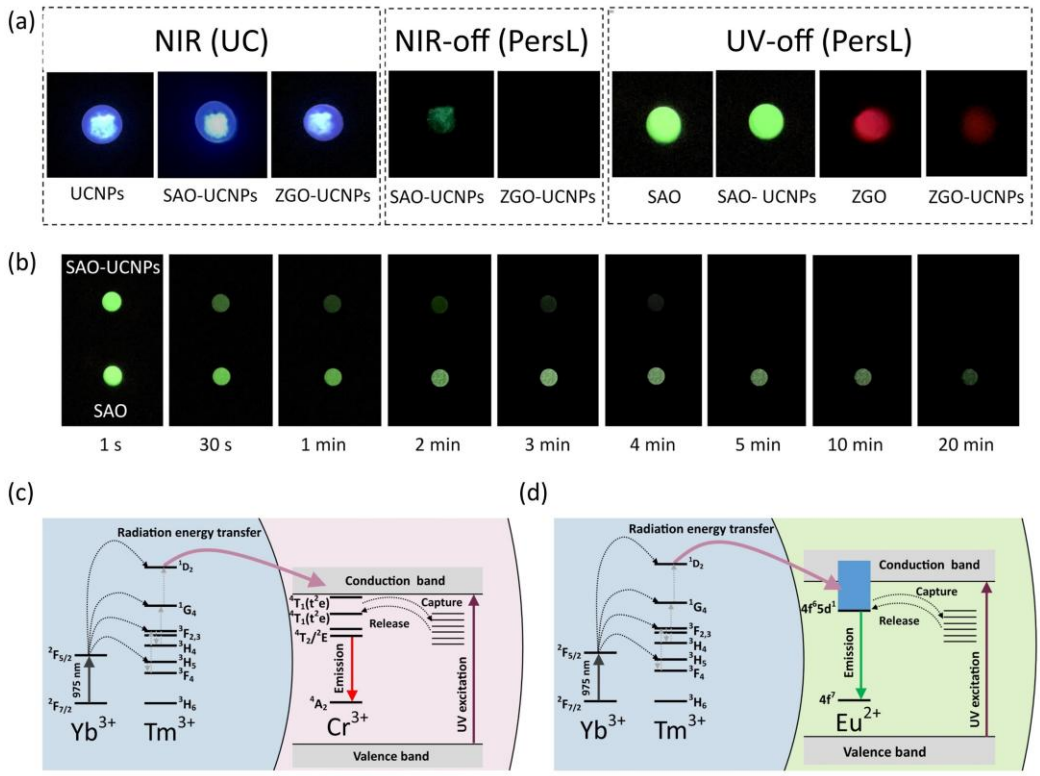

Fig. 5. (a) Emission of $LiYbF_4$:0.5%Tm^{3+}@$LiYF_4$ (UCNPs), $SrAl_2O_4$:Eu^{2+},Dy^{3+} (SAO), $SrAl_2O_4$:1%Eu^{2+},0.5%Dy^{3+}-UCNPs (SAO-UCNPs), $ZnGa_2O_4$:0.5%Cr^{3+} (ZGO) and the composite $ZnGa_2O_4$:0.5%Cr^{3+}-UCNPs (ZGO-UCNPs) under NIR excitation and after (PersL) NIR or UV excitation. (b) Persistent luminescence of SAO and SAO-UCNPs after irradiation with UV light. The photos were taken using an iPhone 13 camera. (c, d) Simplified mechanisms of the observed upconversion and persistent luminescence, showing radiation energy transfer between UCNPs and (c) SAO or (d) ZGO components of composite materials.

Due to the effect of optically stimulated luminescence (OSL), there is a possibility of achieving PersL in the visible spectral range under NIR excitation, which is not a radiation energy transfer from UCNPs.[7] The effect of detrapping electrons under NIR radiation can be misinterpreted as charging PersL with NIR excitation. Therefore, we decided to heat up and then keep the samples in the dark for two days before the measurements and compare the spectroscopic behaviour between the composite materials and the pure PersL phosphors. The materials without UCNPs should not exhibit PersL in the experimental conditions. To confirm

that the observed PersL is not OSL, luminescence decay curves were obtained after 5 mins exposure to NIR laser excitation. This allowed for the assessment of alterations in both decay times and intensities of PersL emission, as illustrated in Fig. S1. Overall, the samples based on the $ZnGa_2O_4:Cr^{3+}$ phosphor show shorter luminescence than those based on $SrAl_2O_4:Eu^{2+},Dy^{3+}$. Composite samples showed intense PersL up to several minutes after switching off the 975 nm laser. Comparison with samples not mixed with UCNPs confirms that NIR radiation charges the samples and that the OSL effect did not induce luminescence.

The final confirmation of the excitation of the PersL phase via upconversion is the recorded emission spectra of SAO, SAO-UCNPs, and ZGO and ZGO-UCNPs samples after the end of irradiation. Fig. 6 shows the time-resolved emission spectra of these samples, acquired after turning the laser or UV diode off with a 1 s interval. Spectra were collected for composite and only-PersL phosphors, allowing us to compare luminescence decays after UV excitation in both materials. It also allows the comparison of UV and NIR-based excitation in the same composite materials. In the case of UV excitation, the persistence luminescence decays are slightly shorter for the composite materials (SAO-UCNPs and ZGO-UCNPs) compared to the pure PersL structures (SAO and ZGO), probably due to the reabsorption effects. Meanwhile, in the case of NIR excitation, the situation is the opposite, i.e., the composite materials exhibit quite longer decays of the afterglow emissions. It may be associated with a more complex excitation mechanism, where pumping of PersL via up-converted photons is required, as well as due to the enhanced energy migration among the emitting ions and traps/defect states within the whole heterostructures.

Additionally, Fig. S2 presents luminescence decays of samples irradiated with a 375 nm UV laser, showing PersL durations of up to 17.2 and 6.4 minutes for SAO and SAO-UCNPs, and 2.5 and less than 1 minute for ZGO and ZGO-UCNPs materials after switching off the UV laser. The decays are much longer than those presented in Figs. 6g and 6h due to differences in the excitation power and detector type, but the trends remain consistent.

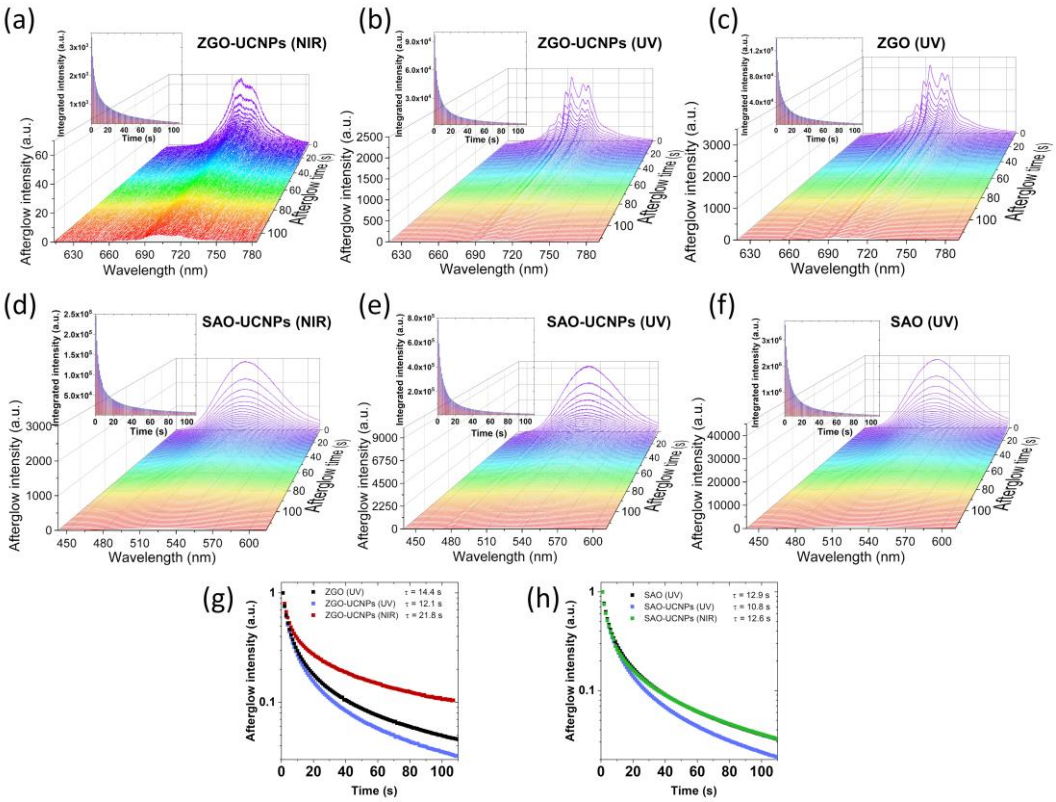

Fig. 6. (a-f) Time-resolved emission spectra of $SrAl_2O_4:Eu^{2+},Dy^{3+}$ (SAO), $SrAl_2O_4:1\%Eu^{2+},0.5\%Dy^{3+}$-UCNPs (SAO-UCNPs), $ZnGa_2O_4:0.5\%Cr^{3+}$ (ZGO) and the composite $ZnGa_2O_4:0.5\%Cr^{3+}$-UCNPs (ZGO-UCNPs) under NIR (only composite samples) and UV excitation; (g, f) normalized luminescence decay curves of the obtained materials measured at the maximum of emission luminescence (520 and 700 nm for Eu^{2+} and Cr^{3+} ions respectively. Measurements were taken using a 375 nm LED and a 975 nm laser with a power density of 6 $W \cdot cm^{-2}$.

3D printing and optical coding

Finally, we have employed the 3D-printing technology to demonstrate the real-world application of the developed multi-modal luminescent materials for advanced optical coding. In all cases, 3 wt.% of the given luminescent materials were initially mixed with the resin precursors, forming semi-transparent, optically active polymer items, 3D-printed with micron-sized resolution (≈50 μm). The leftmost part of Fig. 7 depicts the designed template patterns; the second column shows the corresponding 3D-printed items in daylight, the third column presents the patterns under UV

light irradiation (365 nm), the fourth one shows the afterglow emission of the corresponding pattern (photographs taken just after turning the UV light off). In contrast, the rightmost column (Fig. 7b, c) reveals the patterns under NIR laser exposure (UC emission).

At first, the designed QR code redirecting to the website of our group (www.lanasylum.amu.edu.pl) was 3D-printed using a commercial, transparent resin (cured under UV light), admixed with the Eu^{2+}-activated SAO particles (green emitters) in the form of powder material. The fabricated QR code is hardly observed in daylight, slightly better upon UV light (where the blue emission of polymers obscures green luminescence of Eu^{2+}), and much better in the case of reading in an afterglow mode (Fig. 7a; top). This is thanks to the lack of disturbing background auto-fluorescence (polymer resin emission) or fluorescence of other organic impurities emitting under UV light, which is a great benefit of reading the 3D-printed codes with the afterglow effect. In the same fashion, the acronym words formed by the letters "EDU" and "AMU" were fabricated (Fig. 7a; bottom), which again can be read only in an afterglow mode.

After that, we 3D-printed the 8-bit code utilizing the SAO material for the background units and the combination of the SAO with $LiYbF_4:Tm^{3+}@LiYF_4$ UCNPs (blue emitters) as the active/readable part of the pattern (Fig. 7b). In this case, the designed well-hidden code cannot be read out neither under UV light nor in an afterglow mode, because the whole volume of the fabricated polymer item contains the UV-active component (SAO). On the other hand, using the NIR laser, the securely encrypted 8-bit code can be easily visualized (blue block units) and read as "AFTER@GLOW" *via* ASCII decoding, *i.e.* binary-to-text conversion. Note, in contrast to the powder samples we were unable to detect the green afterglow effect upon NIR laser irradiation of the 3D-printed polymer blocks due to several factors, *i.e.* low laser power density (flux ca. 2 $W \cdot cm^{-2}$) necessary to irradiate the whole pattern, resulting in a relatively low efficiently of the NIR-stimulated afterglow process requiring high excitation flux; strong absorption and scattering of the emitted UV light by the organic polymer material; small amount of the optically active phase in the bulk volume of the fabricated composite.

Based on the results presented, it is clear that using both reading modes, *i.e.* afterglow upon UV excitation and UC under NIR laser, it is possible to increase the security level of the data stored and the information storage capacity per unit volume (density of the optical memories). Hence, to show the proof-of-concept of the next-generation, multi-dimensional coding platform, we developed and 3D-printed the first double-layer codes, which are separately readable with UV and NIR light, as shown in Fig. 7c. In this system, firstly, the UC-active pattern (containing UCNPs) had been 3D-printed as a bottom-layer, and then a second UV-active pattern (made of SAO) exhibiting an afterglow effect has been 3D-printed on top. Each layer has a thickness of around 100 μm, and the bottom layer is entirely invisible by looking from the top, both in daylight and under UV light. By irradiating (from the top) the 3D-printed item with a highly penetrable NIR (975 nm) laser, the blue UC emission of Tm^{3+} can be observed from the ordered 3D-printed units of its bottom layer, which can be decrypted *via* the ASCII coding system as "INFRARED". At the same time, the top layer loads another information, *i.e.* "EMISSION", stored in the form of a different 8-bit code, with the altered arrangement of optically active blocks, clearly readable upon UV light (365 nm) as green afterglow luminescence. In this case, we superimposed some grid lines with the 3D-printed patterns (during image processing) to clarify the revealed optical codes better and facilitate the decoding process. Please note that due to some imperfections of the manufacturing process and limitations of our system for optical imaging, some slight discrepancies may appear between the designed templates and imaged patterns.

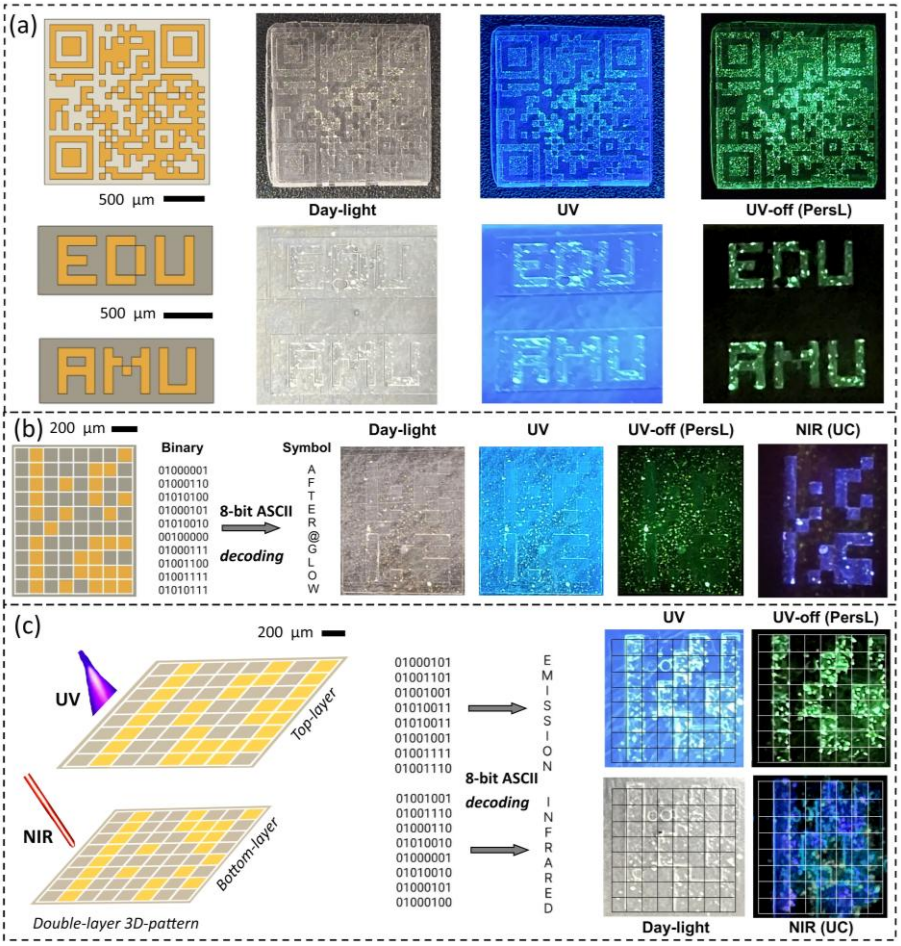

Fig. 7. Multi-dimensional and multi-modal optical coding platform for improved advanced information storage. (a) Micro-structured 3D-printed QR code (top) and letters (bottom) made of Eu^{2+}-activated SAO particles as green emitters (blue emission comes from background auto-fluorescence of polymers), as a template (leftmost), daylight, under UV light (365 nm) and after UV irradiation (light-off) as green persistent (PersL) luminescence. (b) 3D-printed 8-bit code with loaded information "AFTER@GLOW", readable via ASCII decoding of blue UC luminescence revealed under NIR (975 nm) laser irradiation. The pattern contains the UV-active SAO material in its whole volume, including the background part, and the active blocks are made of the mixture of SAO + $LiYbF_4:Tm^{3+}@LiYF_4$ as blue UC emitters. (c) Double-layer, 3D-pattern composed of UV-active SAO (top-layer) and NIR-active LiYbF4:Tm3+@LiYF4 (bottom-layer) components, which can be decoded as "EMISSION" and "INFRARED" by reading in PersL and UC modes, respectively.

Conclusions

We have successfully designed and synthesized new composite materials merging the properties of persistent luminescence phosphors, i.e. $ZnGa_2O_4:Cr^{3+}$ and $SrAl_2O_4:Eu^{2+}$, Dy^{3+} with the properties of upconverting $LiYbF_4:Tm^{3+}@LiYF_4$ core@shell nanoparticles and applied them for the first bi-modal 8-bit coding platform operating in upconversion and afterglow modes. The materials obtained exhibited dual-modal behaviour, demonstrating luminescence under UV excitation in the visible region (at 520 nm for the Eu^{2+}-doped sample) or NIR region (at 700 nm when Cr^{3+} ions were used as dopants) and blue upconversion luminescence when excited at 975 nm. However, the most important feature of these composite materials is that they can also present long-lasting luminescence after being excited with an NIR laser source. This untypical property allows for re-charging the persistent luminescent materials in a medium that is not transparent for UV-Vis excitation light. By combining the unique spectroscopic properties of the developed materials and 3D-printing technology of micron-sized resolution, we fabricated various optically active polymer items (words, QR and 8-bit codes) made of organic resin and phosphor material studied. We successfully showed the development of a genuinely multifunctional coding platform, utilizing afterglow and UC effects alike with the improved density of optical information loading. It was made possible by fabricating the first double-layer 8-bit coding platform with 3D-printed secret codes, which can be read separately with NIR laser and UV light *via* energy up-conversion and afterglow effects, respectively.

Acknowledgements

The presented results were financially supported by the National Science Center Poland (UMO-2021/43/B/ST5/00046) and the Plan Propio de Investigación 2022 of the Universidad de La Laguna through Proyectos Dirigidos por Noveles Investigadores/as (2022/20258).

References

1 P. F. Smet, K. Van den Eeckhout, O. Q. De Clercq and D. Poelman, *Persistent Phosphors*, Elsevier B.V., 1st edn., 2015, vol. 48.

2 Y. Li, M. Gecevicius and J. Qiu, *Chem. Soc. Rev.*, 2016, **45**, 2090–2136.

3 J. Hölsä, *Electrochem. Soc. Interface*, 2009, **18**, 42–50.

4 K. Van den Eeckhout, P. F. Smet and D. Poelman, *Materials (Basel).*, 2010, **3**, 2536–2566.

5 Z. Li, L. Huang, Y. Zhang, Y. Zhao, H. Yang and G. Han, *Nano Res.*, 2017, **10**, 1840–1846.

6 D. Yang, Z., Hu, J., Van der, D., Feng, A., Hu, H., Vrielinck, H., Smet, P. F., Poelman, *Adv. Funct. Mater.*, 2022, **32**, 2201684.

7 D. Van der Heggen, R. Zilenaite, E. Ezerskyte, V. Fritz, K. Korthout, D. Vandenberghe, J. De Grave, J. Garrevoet, L. Vincze, D. Poelman, J. J. Joos and P. F. Smet, *Adv. Funct. Mater.*, , DOI:10.1002/adfm.202109635.

8 A. Bessière, J. O. Durand and C. Noûs, *Nanophotonics*, 2021, **10**, 2999–3029.

9 J. Xue, L. Li, M. Runowski, Y. Guo, B. R. Lee, J. H. Jeong, P. Du and S. H. Park, *Adv. Opt. Mater.*, , DOI:10.1002/adom.202300600.

10 C. Jiang, R. Zhang, L. Han and Y. Chen, *Int. J. Appl. Ceram. Technol.*, 2023, **20**, 3357–3364.

11 Y. Zhuang, L. Wang, Y. Lv, T. L. Zhou and R. J. Xie, *Adv. Funct. Mater.*, 2018, **28**, 1–9.

12 Z. Xue, X. Li, Y. Li, M. Jiang, G. Ren, H. Liu, S. Zeng and J. Hao, *Nanoscale*, 2017, **9**, 7276–7283.

13 L. Huang, L. Lin, W. Xie, Z. Qiu, H. Ni, H. Liang, Q. Tang, L. Cao, J.-X. Meng and F. Li, *Chem. Mater.*, 2020, **32**, 5579–5588.

14 X. Cao, Y. Gong, Y. Li, S. Zhu, X. Zhang, Y. Zhan, F. Kang, J. Wang and J. Liang, *Biomed. Opt. Express*, 2017, **8**, 1466.

15 S. Yu, Z. Wang, R. Cao and L. Meng, *J. Fluor. Chem.*, 2017, **200**, 77–83.

16 L. A. Sordillo, Y. Pu, S. Pratavieira, Y. Budansky and R. R. Alfano, *J. Biomed. Opt.*, 2014, **19**, 056004.

17 N. Jurga, S. Ryszczyńska and T. Grzyb, *Spectrochim. Acta Part A Mol. Biomol. Spectrosc.*,

2023, **303**, 123220.

18 U. Kostiv, Z. Farka, M. J. Mickert, H. H. Gorris, N. Velychkivska, O. Pop-Georgievski, M. Pastucha, E. Odstrčilíková, P. Skládal and D. Horák, *Biomacromolecules*, 2020, **21**, 4502–4513.

19 L. M. Wiesholler, C. Genslein, A. Schroter and T. Hirsch, *Anal. Chem.*, 2018, **90**, 14247–14254.

20 A. Drozdowski, N. Jurga, D. Przybylska, J. C. Brandmeier, Z. Farka, H. H. Gorris and T. Grzyb, *J. Colloid Interface Sci.*, 2023, **649**, 49–57.

21 H. Qiu, M. Tan, T. Y. Ohulchanskyy, J. F. Lovell and G. Chen, *Nanomaterials*, 2018, **8**, 1–18.

22 S. Zha, F. Yang, Z. Ma, H. Wu, D. Zhang and D. Li, *Mater. Des.*, 2023, **226**, 111682.

23 Y. Xie, Y. Song, G. Sun, P. Hu, A. Bednarkiewicz and L. Sun, *Light Sci. Appl.*, , DOI:10.1038/s41377-022-00813-9.

24 M. Runowski, P. Woźny, I. R. Martín, K. Soler-Carracedo, T. Zheng, H. Hemmerich, F. Rivera-López, J. Moszczyński, P. Kulpiński and S. Feldmann, *Adv. Funct. Mater.*, , DOI:10.1002/adfm.202307791.

25 T. Zheng, M. Runowski, J. Xue, L. Luo, U. R. Rodríguez-Mendoza, V. Lavín, I. R. Martín, P. Rodríguez-Hernández, A. Muñoz and P. Du, *Adv. Funct. Mater.*, , DOI:10.1002/adfm.202214663.

26 T. Grzyb, I. R. Martín and R. Popescu, *Nanoscale*, 2024, **16**, 1692–1702.

27 T. Grzyb, D. Przybylska, A. Szczeszak, E. Śmiechowicz, P. Kulpiński and I. R. Martín, *Carbohydr. Polym.*, 2022, **294**, 119782.

28 A. Szczeszak, M. Skwierczyńska, D. Przybylska, M. Runowski, E. Śmiechowicz, A. Erdman, O. Ivashchenko, T. Grzyb, P. Kulpiński and K. Olejnik, *Mater. Des.*, 2022, **218**, 110684.

29 J. Qin, J. Xiang, H. Suo, Y. Chen, Z. Zhang, X. Zhao, Y. Wu and C. Guo, *J. Mater. Chem. C*, 2019, **7**, 11903–11910.

30 Y. Cheng and K. Sun, *J. Fluoresc.*, 2020, **30**, 1251–1259.

31 Y. Cheng, K. Sun and P. Ge, *Opt. Mater. (Amst).*, 2018, **83**, 13–18.

32 N. G. Arango, S. Vuori, H. Byron, D. Van der Heggen, P. F. Smet, M. Lastusaari and L. Petit, *J. Alloys Compd.*, 2022, **927**, 167048.

33 R. E. Rojas-Hernandez, F. Rubio-Marcos, M. V. Dos Santos Rezende, M. Á. Rodriguez, A. Serrano, Á. Muñoz-Noval and J. F. Fernandez, *Mater. Des.*, 2016, **108**, 354–363.

34 R. E. Rojas-Hernandez, F. Rubio-Marcos, M. Á. Rodriguez and J. F. Fernandez, *Renew. Sustain. Energy Rev.*, 2018, **81**, 2759–2770.

35 J. Hölsä, H. Jungner, M. Lastusaari and J. Niittykoski, *J. Alloy. Compd.*, 2001, **323**–**324**, 326–330.

36 F. Clabau, X. Rocquefelte, S. Jobic, P. Deniard, M.-H. Whangbo, A. Garcia and T. Le Mercier, *Chem. Mater.*, 2005, **17**, 3904–3912.

37 J. Kaur, R. Shrivastava, B. Jaykumar and N. S. Suryanarayana, *Res. Chem. Intermed.*, 2014, **40**, 317–343.

38 D. S. Kshatri and A. Khare, *J. Lumin.*, 2014, **155**, 257–268.

39 D. Poelman, D. Van Der Heggen, J. Du, E. Cosaert and P. F. Smet, *J. Appl. Phys.*, , DOI:10.1063/5.0032972.

40 L. Li, Y. Wang, H. Huang, H. Li and H. Zhao, *Mod. Phys. Lett. B*, 2016, **30**, 9–11.

41 T. Lécuyer, N. Bia, P. Burckel, C. Loubat, A. Graillot, J. Seguin, Y. Corvis, J. Liu, L. Valéro, D. Scherman, N. Mignet and C. Richard, *Nanoscale*, 2022, **14**, 1386–1394.

42 J. Shi, X. Sun, S. Zheng, J. Li, X. Fu and H. Zhang, *Biomaterials*, 2018, **152**, 15–23.

43 S. K. Singh, *RSC Adv.*, 2014, **4**, 58674–58698.

44 R. Zou, J. Huang, J. Shi, L. Huang, X. Zhang, K. L. Wong, H. Zhang, D. Jin, J. Wang and Q. Su, *Nano Res.*, 2017, **10**, 2070–2082.

45 Y. E. Serge-Correales, D. Neumeyer, S. Ullah, R. Mauricot, Q. Zou, S. J. L. Ribeiro and M. Verelst, *Langmuir*, 2023, **39**, 1495–1506.

46 L. Song, P. P. Li, W. Yang, X. H. Lin, H. Liang, X. F. Chen, G. Liu, J. Li and H. H. Yang, *Adv. Funct. Mater.*, 2018, **28**, 1–10.

47 W. Fan, N. Lu, C. Xu, Y. Liu, J. Lin, S. Wang, Z. Shen, Z. Yang, J. Qu, T. Wang, S. Chen, P.

Huang and X. Chen, *ACS Nano*, 2017, **11**, 5864–5872.

48 H. Suo, C. Guo, J. Zheng, B. Zhou, C. Ma, X. Zhao, T. Li, P. Guo and E. M. Goldys, *ACS Appl. Mater. Interfaces*, 2016, **8**, 30312–30319.

49 T. Cheng, R. Marin, A. Skripka and F. Vetrone, *J. Am. Chem. Soc.*, 2018, **140**, 12890–12899.

50 A. Skripka, T. Cheng, C. M. S. Jones, R. Marin and F. Vetrone, .

51 H.-W. Chien, M.-T. Tsai, C.-H. Yang, R.-H. Lee and T.-L. Wang, *RSC Adv.*, 2020, **10**, 35600–35610.

52 J. Liu, H. Rijckaert, M. Zeng, K. Haustraete, B. Laforce, L. Vincze, I. Van Driessche, A. M. Kaczmarek and R. Van Deun, *Adv. Funct. Mater.*, 2018, **28**, 1707365.

53 A. Nadort, J. Zhao and E. M. Goldys, *Nanoscale*, 2016, **8**, 13099–13130.

54 B. Zhou, B. Tang, C. Zhang, C. Qin, Z. Gu, Y. Ma, T. Zhai and J. Yao, *Nat. Commun.*, 2020, **11**, 1–9.

55 C. Albrecht, *Anal. Bioanal. Chem.*, 2008, **390**, 1223–1224.

56 A. Skripka, T. Cheng, C. M. S. Jones, R. Marin, J. Marques-Hueso and F. Vetrone, *Nanoscale*, 2020, **12**, 17545–17554.

57 D. Jia, *Opt. Mater. (Amst).*, 2003, **22**, 65–69.

58 P. Scherrer, *Nachr. Ges. Wiss. Göttingen*, 1918, **26**, 98–100.

59 T. Grzyb, A. Szczeszak, Z. Śniadecki, B. Idzikowski and S. Lis, *J. Alloys Compd.*, 2016, **686**, 489–495.

60 a Baran, S. Mahlik, M. Grinberg and E. Zych, *J. Phys. Condens. Matter*, 2013, **25**, 025603.

61 A. Bessière, S. K. Sharma, N. Basavaraju, K. R. Priolkar, L. Binet, B. Viana, A. J. J. Bos, T. Maldiney, C. Richard, D. Scherman and D. Gourier, *Chem. Mater.*, 2014, **26**, 1365–1373.

62 L. P. Sosman, A. D. Tavares, R. J. M. Da Fonseca, T. Abritta and N. M. Khaidukov, *Solid State Commun.*, 2000, **114**, 661–665.

63 Z. Zhou, W. Zheng, J. Kong, Y. Liu, P. Huang, S. Zhou, Z. Chen, J. Shi and X. Chen, *Nanoscale*, 2017, **9**, 6846–6853.

64 X.-H. Lin, L. Song, S. Chen, X.-F. Chen, J.-J. Wei, J. Li, G. Huang and H.-H. Yang, *ACS Appl.*

Mater. Interfaces, 2017, **9**, 41181–41187.

65 M. Misiak, K. Prorok, B. Cichy, A. Bednarkiewicz and W. Stręk, *Opt. Mater. (Amst).*, 2013, **35**, 1124–1128.

66 L. Yang, S. Gai, H. Ding, D. Yang, L. Feng and P. Yang, *Adv. Opt. Mater.*, 2023, **2202382**, 2202382.